Proceedings of the Twenty-first (2011) International Offshore and Polar Engineering Conference
Maui, Hawaii, USA, June 19-24, 2011

ISBN 978-1-880653-96-8 (Set); ISSN 1098-6189 (Set); www.isope.org

Ocean Wave Reconstruction Algorithms Based on Spatio-temporal Data Acquired by a Flash LIDAR Camera

Stéphan T. Grilli[1], *Charles-Antoine Guérin*[2] *and Bart Goldstein*[3]
(1) Department of Ocean Engineering, University of Rhode Island, Narragansett, RI, USA
(2) LSEET Laboratory, CNRS/Université du Sud-Toulon-Var, La Garde, France
(3) Advanced Scientific Concepts, Inc. Santa Barbara, CA, USA

We report on the development of free surface reconstruction algorithms to predict ocean waves, based on spatial observations made with a high frequency ASC Flash LIDAR^{TM} camera. We assume that the camera is mounted on a vessel, in a forward looking position, and is pointing at some distance ahead of its path. In its current design, the camera generates a 64 x 64 matrix of laser rays, providing as many simultaneous measurements of the distance to the ocean surface, every 0.05-0.25 s, in an angular sector of 15-20 by 9-15 deg. (depending on design assumptions). From this data and the camera's location and orientation, the coordinates of the measured surface points can be generated as a function of time; this yields a sample of spatio-temporal wave elevation data. Due to wave shadowing effects, the density of measurement points gradually decreases (i.e., becomes sparse) with the distance to the camera. Free surface reconstruction algorithms were first developed and validated for linear 1D and 2D irregular surface models, whose amplitude coefficients are estimated based on minimizing the mean square error of simulated surface elevations to measurements, over space and time (for a specified time initialization period). In the validation tests reported here, irregular ocean surfaces are generated based on a directional Phillips or JS spectrum, and simulated LIDAR data sets are constructed by performing geometric intersections of laser rays with each generated surface. Once a nowcast of the ocean surface is estimated from the (simulated) LIDAR data, a forecast can be made of expected waves ahead of the vessel, for a time window that depends both on the initialization period and the resolved wavenumbers in the reconstruction. The process can then be repeated for another prediction window, and so forth. To reconstruct severe sea states, however, nonlinear effects must be included in the sea surface representation. This is done, here, by representing the ocean surface using the efficient Lagrangian model Choppy, expressed in a new explicit formulation, which was demonstrated to approximate second-order effects in waves (Nouguier et al., 2009). In the paper, we develop and validate the 1D surface generation and reconstruction of irregular sea states using Choppy.

KEY WORDS: Ocean waves; linear and nonlinear waves; analytical wave models; free surface reconstruction algorithms; flash LIDAR camera.

INTRODUCTION

In many ocean engineering applications, where ocean wave information is needed, it is often sufficient to use phase-averaged wave data, usually in the form of a directional wave energy spectrum. For some applications, however, both more accurate and detailed phase resolved, real time, wave data is required. This is for instance the case for predicting seakeeping and anticipating the motions of a surface vessel, based on measurements of the ocean surface made ahead of its trajectory. In such a case, the free surface must be reconstructed in real time based on measurements, which requires applying so-called free surface reconstruction algorithms.

Here, we report on the development of such algorithms to predict the ocean surface based on spatio-temporal data, acquired at a high frequency by a Flash LIDAR^{TM} camera (designed by Advanced Scientific Concepts, Inc.; Santa Barbara, California, USA). The camera is mounted on a vessel (on top of a mast), in a forward looking position, and is pointing at some distance ahead of its path. In its currently planned design, the camera will generate a 64 x 64 matrix of laser rays, providing as many simultaneous measurements of the distance to the ocean surface. From this data and the cameras location and orientation, the elevation and horizontal position of the measured surface points can be generated in an absolute coordinate system.

A shallow angle (vessel mounted) LIDAR scanning system was already proposed by Belmont et al. (2006), and field tested for wave profiling up to distances of hundreds of meters, for one-dimensional (1D) cases (i.e., in a vertical plane). As indicated by the authors, as laser rays are first reflecting off of the nearest ocean wave crests (due to wave shadowing effects), the density of measurement points gradually decreases with the distance to the camera. Hence, this results in a highly spatially non-uniform distribution of wave elevation values/data (as e.g. sketched in Fig. 1). To alleviate this problem, Belmont (2007) proposed a remapping technique of such 1D data onto a uniform spatial grid. This method was tested with some success, for 1D cases, in the present work, but was found to be hard to use and less accurate for two-dimensional (2D) cases. Instead, an alternate approach for "enriching" LIDAR data sets of wave surface elevation was developed and shown to be effective in both 1D and 2D, based on using spatio-temporal data in the free surface reconstruction algoritms, rather than purely spatial data. This is detailed later.

In the following sections, we present the development and validation of new free surface reconstruction algorithms based on a linear or 2nd-order representation of 1D and 2D irregular ocean surfaces, whose

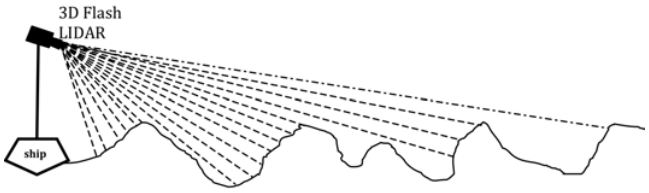

Fig. 1: Sketch of flash-LIDAR angle of view of the ocean surface and visualization of a few rays (1D situation). Measurement points are sparse far from the ship.

parameters are estimated based on minimizing the mean-square error of simulated surface elevations to measurements, over space and time (for a specified time prediction window). Once sea state is properly estimated, a prediction of expected waves ahead of the vessel can be made; the process is then repeated for another prediction window, and so forth.

While a linear reconstruction should be sufficient for the short term forecast of moderate sea states, to better estimate more severe sea states, nonlinear effects must be included in the sea surface representation. The use of 2nd- and 3rd-order (and even higher-order) free surface models in reconstruction algorithms was investigated by Wu (2004), Blondel (2009), and Blondel et al. (2010). The proposed nonlinear models, however, were all quite computationally demanding, particularly in a reconstruction mode. Here, we represent nonlinear sea surfaces using the efficient Lagrangian model Choppy, which was demonstrated to correctly approximate second-order properties of waves with narrow-banded spectra (Nouguier et al., 2009). A new, more efficient, explicit formulation of this model is developed and used in the reconstruction algorithms, which is shown to be accurate enough for most sea states.

OCEAN FREE SURFACE REPRESENTATION

In this work, the ocean surface representation will be either based on linear superposition (Dean and Dalrymple, 1984) or on the nonlinear Choppy wave model, which is an extension of Gertsner's wave theory (Nouguier et al., 2009), expressed in a new explicit formulation, which makes it an efficient means of generating synthetic ocean surface with adequate second-order properties. As a reminder, linear Stokes wave theory shows that for any wave harmonic of wavenumber k_n (wavelength λ_n) and circular frequency ω_n, (period T_n), the dispersion relationship,

$$\frac{\omega_n^2}{g} = k_n \tanh k_n h \quad \text{with} \quad \omega_n = \frac{2\pi}{T_n} \;\; ; \;\; k_n = \frac{2\pi}{\lambda_n} \tag{1}$$

and group velocity formulation,

$$c_{gn} = \frac{d\,\omega_n}{d\,k_n} = \frac{g}{2\omega_n} \tanh k_n h \left\{ 1 + \frac{2k_n h}{\sinh 2k_n h} \right\} \tag{2}$$

hold at second-order (in water depth h, where g denotes the gravitational acceleration). Amplitude dispersion effects, not included in these equations, only appear at 3rd-order or higher. Other characteristics, such as wave crest and trough elevations, wave slopes, differ at second-order. In deep water, Eqs. (1) and (2) simplify to: $\omega_n^2 = g k_n$ and $c_{gn} = g/(2\omega_n)$.

Hence, the linear superposition, for $(n = 1, \ldots, N)$, of individual wave harmonics of elevation A_n and direction Θ_n yields the linear ocean surface representation, in the plane $\boldsymbol{x} = (x, y)$,

$$\eta_{\text{L}}(\boldsymbol{x}, t) = \sum_{n=1}^{N} A_n \cos\left(\Psi_n - \varphi_n\right) \;\; ; \;\; \Psi_n = k_{nx} x + k_{ny} y - \omega_n t \tag{3}$$

where Ψ_n are spatio-temporal phase functions, $\varphi_n = 2\pi \mathcal{R}_n$ are mutually independent (i.e., random) phases, with $\mathcal{R}_n \in [0, 1]$ a set of uniformly distributed random numbers. Note, one can also denote, $(k_{xn}, k_{yn}) = k_n\{x \cos\Theta_n + y \sin\Theta_n\} = \boldsymbol{k}_n \cdot \boldsymbol{x}$, with $\boldsymbol{k}_n = k_n(\cos\Theta_n, \sin\Theta_n) = k_n \hat{\boldsymbol{k}}_n$, with $\hat{\boldsymbol{k}}_n = (\cos\Theta_n, \sin\Theta_n)$, the unit wavenumber vector.

To simplify the following mathematical and algorithm developments, related to free surface reconstruction, it is more convenient (and accurate) to use the equivalent linear representation,

$$\eta_{\text{L}}(\boldsymbol{x}, t) = \sum_{n=1}^{N} k_n^{-3/2} \left\{ a_n \cos\Psi_n + b_n \sin\Psi_n \right\} \tag{4}$$

where $\{a_n, b_n; n = 1, \ldots, N\}$ are $2N$ wave harmonic parameters describing the ocean surface, with,

$$a_n = A_n \cos\varphi_n \;\; ; \;\; b_n = A_n \sin\varphi_n \tag{5}$$

The factors $k_n^{-3/2}$ constitute a preconditioning, which anticipates the fact that the harmonic amplitude coefficients are related to the square root of the energy density spectrum (see below). This preconditioning will make for better conditioned matrices in the reconstruction algorithms discussed later.

The Choppy ocean surfaces are obtained from linear surfaces, such as Eq. (3), based on the transformation,

$$(\boldsymbol{x}, \eta(\boldsymbol{x}, t)) \rightarrow (\boldsymbol{x} + \boldsymbol{D}(\boldsymbol{x}, t), \eta(\boldsymbol{x}, t)) \tag{6}$$

where $\boldsymbol{D}(\boldsymbol{x}, t)$ is the spatial Riez Transform (Hilbert Transform in 1D) of η. It can be shown (Nouguier et al., 2009) that this transformation introduces a phase quadrature with respect to the original signal; hence, it writes,

$$\boldsymbol{D}(\boldsymbol{x}, t) = \sum_{n=1}^{N} k_n^{-3/2} \left\{ -a_n \sin\Psi_n + b_n \cos\Psi_n \right\} \hat{\boldsymbol{k}}_n \tag{7}$$

The nonlinear surface, η_{NL} is thus implicitly defined as,

$$\eta_{\text{NL}}(\boldsymbol{x} + \boldsymbol{D}(\boldsymbol{x}, t), t) = \eta_{\text{L}}(\boldsymbol{x}, t) \tag{8}$$

The horizontal displacement $\boldsymbol{D}$ is assumed small, so that there are no multiple-valued points in the abscissa transformation and the correspondence between η_{NL} and η_{L} is univocal, i.e., for instance in 1D, there exists an increasing function $\xi = \Phi(x)$ such that $x = \xi + D(\xi)$. This is the case if the condition $\mid D' \mid < 1$ is satisfied, which imposes a restriction on the ocean surface slopes, since D and η can easily be shown to have the same RMS slope. In such a case, Eq. (8) can be made explicit, providing the approximation,

$$\eta_{\text{NL}}(\boldsymbol{x}, t) \simeq \eta_{\text{L}}(\boldsymbol{x} - \boldsymbol{D}(\boldsymbol{x}, t), t) \tag{9}$$

which yields the explicit Choppy free surface representation,

$$\eta_{\text{NL}}(\boldsymbol{x}, t) = \sum_{n=1}^{N} k_n^{-3/2} \left\{ a_n \cos\Psi'_n + b_n \sin\Psi'_n \right\} \tag{10}$$

$$\Psi'_n = \boldsymbol{k}_n \cdot (\boldsymbol{x} - \boldsymbol{D}(\boldsymbol{x}, t)) - \omega_n t = \Psi_n - \boldsymbol{k}_n \cdot \boldsymbol{D}(\boldsymbol{x}, t) \tag{11}$$

One can assess the accuracy of this approximation, for instance in 1D, by calculating,

$$\begin{aligned} \mid \eta_{\text{NL}}(x) \;-\; & \eta(x - D(x)) \mid = \mid \eta(\xi) - \eta(x - D(x)) \mid \\ = \;& \mid \eta(x - D(x - D(\xi))) - \eta(x - D(x)) \mid \\ \leq \;& \sup \mid \eta' \mid \mid D(x - D(\xi)) - D(x) \mid \\ \leq \;& \sup \mid \eta' \mid \sup \mid D' \mid \mid D(\xi) \mid \end{aligned} \tag{12}$$

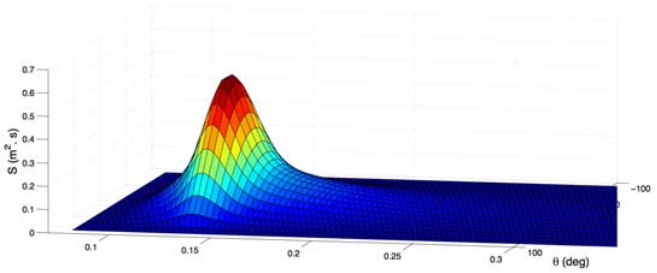

Fig. 2: Directional JS frequency spectrum for significant wave height $H_s = 2$ m and peak spectral period $T_p = 7.5$ s, with spreading exponent $s = 2$ (angular variation $\Theta \in [-90, 90]$ deg.), $\Theta_0 = 0$ and $\varepsilon = 0.05\%$.

which shows that the relative error in Eq. (9) is on the order of the mean square slope (i.e., less than 5% for typical ocean surfaces).

In the ocean, we assume that the wave amplitude of each component can be found from a (discretized) directional energy density spectrum $S(k_n, \Theta_n)$ or $S(\omega_n, \Theta_n)$ (these two forms being related through Eq. (1)), as

$$A_n = \sqrt{2\, S(k_n, \Theta_n)\, \Delta k\, \Delta\Theta} \tag{13}$$

In the following applications, when generating ocean surfaces (whether linear or nonlinear), we will either assume an omnidirectional discrete Phillips spectrum (PS),

$$S(k_n, \Theta_n) = \alpha k_n^{-3} \;\text{ and }\; \lambda_{max} = 8.6\frac{U_{10}^2}{g} \tag{14}$$

(with maximum wavenumber $k_{max} = 2\pi/\lambda_{max}$) function of wind speed at 10 m, U_{10}, and $\alpha = 0.005$; or a directional JONSWAP spectrum (JS), with similar high frequency tail, but more complex variation at lower frequency, function of a peak spectral period T_p ($\omega_p = 2\pi/T_p$ is the peak spectral circular frequency) and peakedness γ (typically $\simeq 3.3$), and an analytic directional spreading function $\mathcal{D}(\Theta, \Theta_o)$,

$$S(\omega, \Theta) = \alpha \frac{g}{\omega^5} \exp\left\{ -\frac{5}{4}\left(\frac{\omega_p}{\omega}\right)^4 \right\} \gamma^r\, \mathcal{D}(\Theta, \Theta_o) \tag{15}$$

$$r = \exp\left\{ -\frac{(\omega_p - \omega)^2}{2\sigma^2\omega_p^2} \right\} \quad \text{and} \quad \mathcal{D} = \mathcal{S} \cos^s(\Theta - \Theta_o) \tag{16}$$

with $\sigma = 0.07$ ($\omega \leq \omega_p$) and $\sigma = 0.09$ ($\omega > \omega_p$), $\mathcal{S}$ a scaling coefficient equal to the inverse of the integral of $\mathcal{D}$ over the angular domain (e.g., $2/\pi$ for $s = 2$). JS is a two parameters spectrum, usually wind speed at 10 m, U_{10} and fetch F in direction Θ_o, with according to Hasselman's parameterization,

$$\alpha = 0.076\left(\frac{U_{10}^2}{gF}\right)^{0.22} \quad \text{and} \quad \omega_p = 22\left(\frac{g^2}{U_{10}F}\right)^{0.33} \tag{17}$$

For PS or JS spectra, the sea state significant wave height is related to the zero-th spectral moment m_o as,

$$H_s = 4\sqrt{m_o} \;;\; m_o = \sigma^2 = \sum_{n=1}^{N} S(k_n, \Theta_n) \Delta k_n \Delta\Theta \tag{18}$$

where σ denotes the standard deviation of the ocean free surface. Combining Eqs. (16)-(18), one can also generate a JS spectrum for specified (H_s, T_p) values.

In the free surface generation using PS or JS spectra, one sets lower and higher frequency or wavenumber cutoff values (k_{min}, k_{max}) and uses N wavenumbers k_n, defined on a logarithmic scale in between these values. For PS spectra, in addition to the maximum wavenumber in (14), one uses $L_{min} = 1$ m. For JS spectra, one selects the cutoff values on the basis of a minimum spectral energy threshold, which is a small fraction (e.g., $\varepsilon = 0.0005$) of the peak spectral value. Fig. 2 shows an example of a directional JS spectrum, for significant wave height $H_s = 2$ m, peak spectral period $T_p = 7.5$ s, spreading exponent $s = 2$ (angular variation $\Theta \in [-90, 90]$ deg.), $\Theta_0 = 0$, and $\varepsilon = 0.05\%$.

FREE SURFACE RECONSTRUCTION ALGORITHMS

Assuming a set of observations of the free surface elevation made at M times, using a LIDAR camera with J active rays (i.e., actually intersecting the free surface), i.e., $\eta_{j,m} = \eta(\boldsymbol{x}_j, t_m); l = j, \ldots, J; m = 1, \ldots, M$, one wishes to reconstruct the ocean surface geometry over some specified range of wavelengths: $(\lambda^r_{min}, \lambda^r_{max})$. In the following, we present reconstruction algorithms based on a linear or Choppy representation of the free surface. These consist in optimizing the values of $2N$ unknown parameters (a_n, b_n), by minimizing a cost function expressing the Root Mean Square (RMS) difference between the reconstructed surface values and the observations.

Due to lack of actual data at this time, we validate the proposed algorithms using numerically simulated LIDAR data on the basis of randomly generated ocean surfaces on the basis of a specified wave energy spectrum, obtained as detailed in the above section (i.e., linear or Choppy). In the validation applications, both 1D (linear or Choppy) and 2D linear cases will be presented in this paper. This is detailed later.

Linear Ocean Free Surface Reconstruction

Here, we assume that the observed ocean surface can be represented by Eq. (4). The simplest minimization of differences between model and observations can be achieved through applying a straightforward Least Square Method (LSM). We first define a cost function for the measured spatio-temporal data points $l = 1, \ldots, L = J \cdot M$ as,

$$C = \frac{1}{L}\sum_{l=1}^{L} (\tilde{\eta}_l(\boldsymbol{x}_l, t_l) - \eta_l)^2 \tag{19}$$

where $\tilde{\eta}_l(\boldsymbol{x}_l, t_l)$ are the unknown reconstructed surface elevations and η_l are the observations. An extremum of this function is reached for,

$$\frac{\partial C}{\partial a_m} = 0, \; \frac{\partial C}{\partial b_m} = 0 \;;\; m = 1, .., N \tag{20}$$

Elementary algebra leads to the following linear system of equations for the unknown parameters, for ($m = 1, \ldots, N$),

$$\begin{aligned}
\sum_{l=1}^{L}\sum_{n=1}^{N} k_n^{-3/2}\{a_n \cos\Psi_{ml}\cos\Psi_{nl} \;+\; b_n \cos\Psi_{ml}\sin\Psi_{nl}\} &= \sum_{l=1}^{L} \eta_l \cos\Psi_{ml} \\
\sum_{l=1}^{L}\sum_{n=1}^{N} k_n^{-3/2}\{a_n \sin\Psi_{ml}\cos\Psi_{nl} \;+\; b_n \sin\Psi_{ml}\sin\Psi_{nl}\} &= \sum_{l=1}^{L} \eta_l \sin\Psi_{ml}
\end{aligned} \tag{21}$$

where wave harmonic phases are defined as, $\Psi_{nl} = \boldsymbol{k}_n \cdot \boldsymbol{x}_l - \omega_n t_l$. There are $2N$ unknowns in these $2N$ equations. This linear system can be recast in matrix form as,

$$A_{mn} X_n = B_n \;;\; X_n = [a_1..a_N, b_1..b_N] \tag{22}$$

where X_n is the vector made of the $2N$ unknown parameters, and B_n is the vector,

$$B_m = \left\{ \begin{array}{l} \sum_{l=1}^{L} \eta_l \cos\Psi_{ml};\ 1 \le m \le N \\ \sum_{l=1}^{L} \eta_l \sin\Psi_{ml};\ N+1 \le m \le 2N \end{array} \right\} \quad (23)$$

and A_{mn} is the $2N \times 2N$ matrix, for $1 \le m, n \le N$,

$$\begin{aligned} A_{mn} &= \sum_{l=1}^{L} k_n^{-3/2} \cos\Psi_{ml} \cos\Psi_{n,} \\ A_{m,N+n} &= \sum_{l=1}^{L} k_n^{-3/2} \cos\Psi_{ml} \sin\Psi_{nl} \\ A_{N+m,n} &= \sum_{l=1}^{L} k_n^{-3/2} \sin\Psi_{ml} \cos\Psi_{nl} \\ A_{N+m,N+n} &= \sum_{l=1}^{L} k_n^{-3/2} \sin\Psi_{ml} \sin\Psi_{nl} \end{aligned} \quad (24)$$

The linear system (22) is solved at each time step of data acquisition (for data acquired at this and $M-1$ earlier time steps), using either the direct Gauss elimination method or, for larger systems, the more efficient iterative method GMRES, with the solution at each time t being initialized using the converged solution at time $t - \Delta t$ (where Δt is the time step for free surface reconstruction).

Choppy Ocean Free Surface Reconstruction

Here, we assume that the observed ocean surface can be represented by Eq. (10), using the definition Eqs. (7) of $\boldsymbol{D}$. As before, we use a quadratic cost function to optimize the reconstructed surface amplitude parameters (a_n, b_n) with respect to $L = M \cdot J$ spatio-temporal observations, as,

$$C = \frac{1}{L} \sum_{l=1}^{L} (\tilde{\eta}_{\text{NL}}(\boldsymbol{x}_l, t_l) - \eta_l)^2 \quad (25)$$

The extremum condition is the same as Eq. (20), but now results in a more complicated nonlinear system of equations for the unknown amplitude coefficients,

$$\sum_{l=1}^{L} \sum_{n=1}^{N} k_n^{-3/2} \{a_n P_{ml} \cos\Psi'_{nl} + b_n P_{ml} \sin\Psi'_{nl}\} = \sum_{l=1}^{L} \eta_l P_{ml}$$

$$\sum_{l=1}^{L} \sum_{n=1}^{N} k_n^{-3/2} \{a_n Q_{ml} \cos\Psi'_{nl} + b_n Q_{ml} \sin\Psi'_{nl}\} = \sum_{l=1}^{L} \eta_l Q_{ml}$$

with,

$$\begin{aligned} P_{ml} = \frac{\partial \eta_{\text{NL}\,l}}{\partial a_m} &= (1 + b_m k_m^{-1/2} \sin\Psi_{ml}) \cos\Psi'_{ml} \\ &- a_m k_m^{-1/2} \sin\Psi_{ml} \sin\Psi'_{ml} \\ Q_{ml} = \frac{\partial \eta_{\text{NL}\,l}}{\partial b_m} &= (1 + a_m k_m^{-1/2} \cos\Psi_{ml}) \sin\Psi'_{ml} \\ &- b_m k_m^{-1/2} \cos\Psi_{ml} \cos\Psi'_{ml} \end{aligned} \quad (26)$$

with the earlier definitions (3), (11) of Ψ and Ψ'.

Similarly to the linear reconstruction, these equations can be recast in the matrix form of Eq. (22), with,

$$B_m = \left\{ \begin{array}{l} \sum_{l=1}^{L} \eta_l P_{ml},\ 1 \le m \le N \\ \sum_{l=1}^{L} \eta_l Q_{ml},\ N+1 \le m \le 2N \end{array} \right\} \quad (27)$$

and, for $1 \le m, n \le N$,

$$\begin{aligned} A_{mn} &= \sum_{l=1}^{L} k_n^{-3/2} P_{ml} \cos\Psi'_{nl} \\ A_{m,N+n} &= \sum_{l=1}^{L} k_n^{-3/2} P_{ml} \sin\Psi'_{nl} \\ A_{N+m,n} &= \sum_{l=1}^{L} k_n^{-3/2} Q_{ml} \cos\Psi'_{n,l} \\ A_{N+m,N+n} &= \sum_{l=1}^{L} k_n^{-3/2} Q_{ml} \sin\Psi'_{nl} \end{aligned} \quad (28)$$

To solve the nonlinear system of Eqs. (22), (27), and (28), we proceed iteratively. Starting from the solution (a_n^0, b_n^0) (i.e., for $i = 0$) of the linear system of Eqs. (22), (23), and (24), we then use for the next iteration in Eq. (26),

$$\Psi'^{i+1}_{ml} \simeq \Psi'^{i}_{ml}\ ;\ P^{i+1}_{ml} \simeq P^{i}_{ml}\ ;\ Q^{i+1}_{ml} \simeq Q^{i}_{ml} \quad (29)$$

where the right-hand-side values are calculated using coefficients (a_m^i, b_m^i), and so forth until convergence. This approximation linearizes the nonlinear system with respect to the amplitude coefficients. In the applications, it is observed that convergence is usually achieved within two iterations.

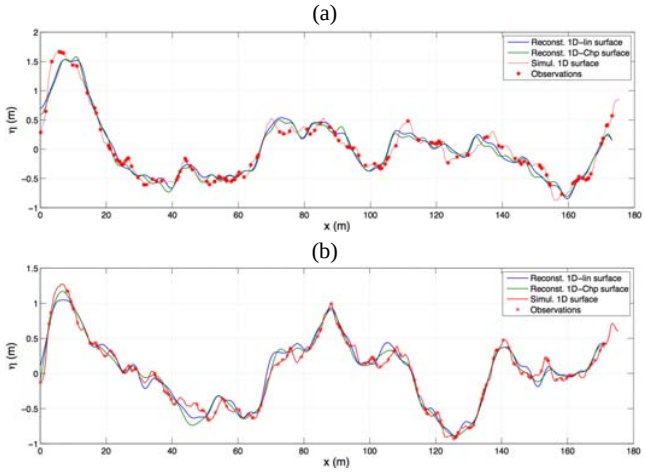

Fig. 3: Application of 1D free surface reconstruction algorithms to a randomly sampled Choppy irregular sea surface (Phillip's spectrum, for $U_{10} = 10$ m/s, $H_s \simeq 2$ m, generated using 20 frequencies). (a) Using spatial data at one time step $t = 0$ (13 frequencies); (b) Using spatio-temporal data at 5 time steps (18 frequencies), for $t = 0.45$ s.

APPLICATIONS

Generation and Reconstruction Using 1D Random Data

Figure 3 shows the application of linear and nonlinear (Choppy) reconstruction algorithms, to a randomly sampled 1D ocean surface generated using Choppy, based on a Phillips spectrum with $U_{10} = 10$ m/s (Eq. (14)). This yields $H_s \simeq 2$ m (Eq. (18)), and $L_{max} \simeq 87$ m or $T_p \simeq 7.5s$ in deep water. We simulate the free surface, using $N = 20$ harmonics with logarithmically spaced wavenumbers, $k_n \in [0.07, 6.3]$ m^{-1}, i.e.,

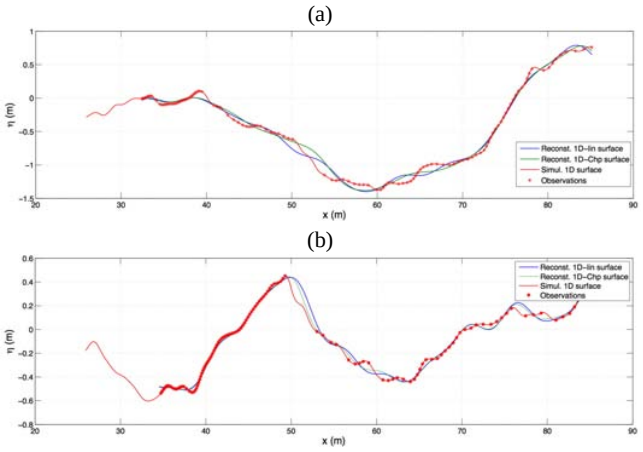

Fig. 4: Application of 1D free surface reconstruction algorithms to a LIDAR-like sampled Choppy irregular sea surface (JS spectrum, for $H_s = 2$ m, $T_p = 7.5$ s, using 320 frequencies). (a) Using spatial data at one time step (8 frequencies); (b) Using spatio-temporal data at 5 time steps (11 frequencies).

wavelengths $\lambda = 1$ to 87 m. The corresponding scaled amplitude coefficients (a_n, b_n) to be used for simulating the free surface are randomly selected using Eqs. (5) and (13) with $\varphi_n = 2\pi\mathcal{R}_n$.

Free surfaces are generated and then propagated in time using Eqs. (4),(5) and (7)-(11), for linear or Choppy cases, respectively. A series of $L = 128$ observations of free surface elevation η_l are then randomly selected on the simulated ocean surface, over abscissa $x_l = 0$ to $2\lambda_{max} = 172$ m, for $t = 0$ to $9\Delta t$, with $\Delta t = 1/f_L = 0.05$ s. No additional noise, representing experimental errors, is included at this stage. These data points are used to apply both the linear and Choppy free surface reconstruction algorithms. In a first test (Fig. 3a), we only use spatial data at one time step ($t = 0$) in the LSM minimization, i.e., $L = 128$. In a second test (Fig. 3b), we use spatio-temporal data from 5 successive time steps in the LSM minimization, i.e., $L = 640$.

After some trial and errors, to ensure both convergence and accuracy of the results, we specify a number of wavenumbers k_n for the Choppy reconstruction equals to 1/10th or 1/40th the number of observations in the first or second tests, or $N = 13$ or 18, respectively, corresponding to as many pairs of unknown coefficients (a_n, b_n). [Note, it appears that one needs to reduce the number of coefficients in the Choppy reconstruction, as compared to a linear reconstruction, in order to obtain a stable solution. This might be related to stability conditions of the iterative solution of the Choppy nonlinear system of equations.] These wavenumbers are also selected logarithmically spaced in a specified useful range, i.e., here corresponding to wavelengths $\lambda_n \in [5, 87]$ m, which removes the highest frequencies from the reconstruction. The LSM optimization algorithm is applied, which provides coefficient values and allows reconstructing the estimated free surface (together with the selected wavenumbers).

In Fig. 3 we compare the reconstructed linear or Choppy free surfaces to the Choppy surfaces generated at the same time. We see, the reconstructed surfaces both capture well the salient features of the actual ocean surfaces, above the 5 m wavelength selected as the higher frequency cut-off in the algorithm. As expected, the nonlinear surface has sharper crests and wider troughs than the linear surface. In the first test (a), the RMS difference between reconstructed and initial Choppy surfaces is $0.063H_s = 0.126$ m (with $0.07H_s$ for the linear reconstruction). In the second test (b), this difference is only in average $0.049H_s = 0.098$ m (and $0.054H_s$ for the linear reconstruction) for 5 successive time steps of reconstruction, each using 5 time steps of data (i.e., the current and four earlier ones). This can be considered as good.

Generation and Reconstruction using 1D LIDAR Data

Here, we apply the reconstruction algorithms to the more realistic case of an irregular ocean surface corresponding to a JONSWAP energy density spectrum (Eqs. (15)-(17)), with significant wave height $H_s = 2$ m and peak spectral period $T_p = 7.5$ s (as for the earlier Phillips spectrum), and $\Theta = \Theta_o = 0$ (e.g., Fig. 2 for $s = 0$). The spectrum has been cut-off in the lower and higher frequency ranges where the energy density falls below 0.005% of the spectral peak. This yields a circular frequency range, $\omega = 0.50 - 6.28$ r/s. Ocean surfaces are generated based on this spectrum, as before, using a random phase method. Here, we use 320 individual frequencies over the selected frequency range; corresponding wavenumbers are calculated using the linear dispersion relationship (1): assuming deep water waves, we have, $k_n = \omega_n^2/g$, which yields $k_n = 0.026 - 4.04$ m^{-1} or wavelengths varying from 1.56 to 244 m.

We then create a simulated LIDAR data set by calculating the geometric intersections of LIDAR rays with the simulated free surfaces as a function of space and time (e.g., Fig. 1). In the following, we assume that the camera is located at $x_0 = 0$, $z_0 = 7.5$ m; the LIDAR main axis of view points at a distance $d_0 = 50$ m ahead; the vertical aperture is $\theta_v = 9$ deg.; there are $n_{rv} = 128$ rays in the vertical plane; the LIDAR acquires simultaneous data at a 20 Hz frequency (i.e., every 0.05 s).

Figure 4 shows results of the application of the interface reconstruction algorithm to 0.25 s worth of simulated LIDAR data obtained from a Choppy ocean surface generated at times $t = 0 - 0.45$ s. No additional noise, representing experimental errors, is included at this stage. For the selected geometry and LIDAR parameters, 117 to 122 data points $(x_l(t), \eta(x_l(t)))$ (i.e., $l = 1, \ldots, L = 117 - 122$) are obtained on the free surface at each time step (e.g., as shown on the figure for time $t = 3$ s) and a new set of coefficients (a_n, b_n) is calculated based on those, for each selected time (i.e., here for 10 surface realizations over 0.45 s). These data points are used in the linear free surface reconstruction algorithm. In a first test, we only use spatial data for one time step at a time in the LSM minimization, i.e., $L = 117 - 122$. In a second test, we use spatio-temporal data from 5 successive time steps in the LSM minimization, i.e., $L = 585 - 610$.

After some trials and errors, we specify a number of wavenumbers k_n for the reconstruction equals to 1/15th or 1/60th the number of observations in the first or second test, or $N \simeq 8 - 9$ or 11-12, corresponding to as many pairs of unknown coefficients (a_n, b_n). These wavenumbers are selected logarithmically spaced in the USV expected useful range $\in [0.08, 1.25]$ m^{-1}, i.e., wavelength $\lambda_n = 5$ to 80 m. The LSM optimization algorithm is applied, which provides values of these coefficients and allows reconstructing the estimated free surface (on the basis of the selected wavenumbers).

Figure 4 shows the reconstructed free surface for these 2 tests (the latter for $t = 0.45$ s), as compared to the initially simulated surfaces. We see, despite the paucity of data for the more distant waves (which is an expected characteristics of LIDAR data) and particularly behind wave crests, as for purely random data selection, the reconstructed surfaces capture well the salient features of the actual ocean surfaces, above the 5 m wavelength selected as the higher frequency cut-off in the algorithm. In the first test (a), the RMS difference between reconstructed and initial surfaces using Choppy is $0.033H_s = 0.066$ m (averaged over 10 time steps; the corresponding difference is $0.034H_s$ using linear reconstruction). In the second test (b), this difference is only in average $0.024H_s = 0.048$ m, averaged for 5 successive time steps of reconstruction, each using 5 time steps of data (the current one and 4 earlier

ones); this difference is $0.029H_s$ using linear reconstruction. This can be considered as quite good as confirmed by visual observation. Only the higher-frequency waves, below the selected 5 m wavelength cutoff, are not well reconstructed.

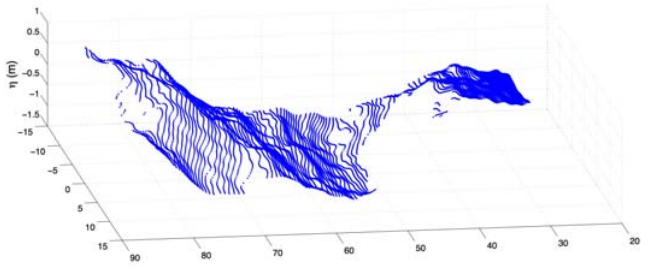

Fig. 5: Typical simulated 2D-LIDAR data for 128 x 128 rays (15,063 actual data points), with the camera located at $x_0 = 0$, $z_0 = 7.5$ m, and a vertical aperture $\theta_v = 9$ deg. and horizontal aperture $\theta_h = 20$ deg. Note the large number of missing data points behind the first wave crest, due to shadowing effects.

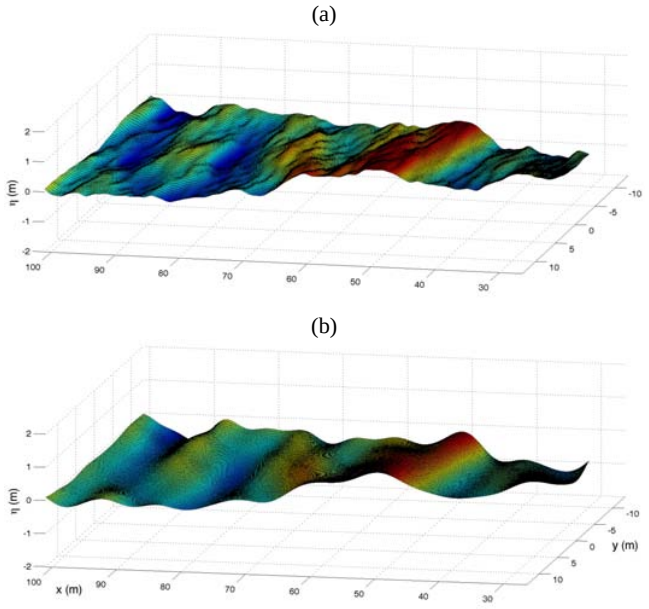

Fig. 6: (a) Simulated and (b) reconstructed ocean surfaces at $t = 1.25$ s, using 2D-LIDAR data for 64 x 64 rays ($L = 23,141$ LIDAR observations for 6 time frames, for $t = 0 - 1.25$ s).

Reconstruction and Forecast using 2D LIDAR Data

Forecasting 2D ocean surfaces on the basis of reconstruction with LIDAR data is the main goal of this work. To validate the 2D algorithms in this respect, we have slightly adjusted the LIDAR camera parameter down to a minimum configuration ($n_{rv} = n_{rh} = 64$ x 64 rays; i.e., there are 4,096 LIDAR rays) and frequency of data acquisition (4Hz; $\Delta t = 0.25$ s), which should represent an achievable hardware in a near-future. The camera is located at $x_0 = 0$, $z_0 = 10$ m, with its main axis of view pointing at a distance $d_0 = 50$ m ahead; the vertical aperture is $\theta_v = 13$ deg. and the horizontal aperture is $\theta_h = 15$ deg.

We randomly generate linear 2D surfaces, on the basis of a JS directional energy density spectrum, with $s = 2$, $\Theta_0 = 0$, and a spreading angle discretization of 10 deg., from -90 deg. to +90 deg. We again use a significant wave height $H_s = 2$ m and peak spectral period $T_p = 7.5$ s (Fig. 2). Other parameters N and k_n are as before. The latter are projected over each spectral direction Θ to yield wavenumber vectors (k_{nx}, k_{ny}). The LIDAR ray intersections with the free surface are successively calculated in each vertical plane; Fig. 5 shows an example of simulated 2D-LIDAR data points.

We create a simulated 2D LIDAR data set for 6 time frames of ocean surface, from $t = 0 - 1.25$ s; this yields a total of $L = 23,141$ simulated LIDAR observations. Figure 6 shows the linearly generated and reconstructed surfaces at $t = 1.25$ s, using this LIDAR data. Based on earlier tests, we use $N = 15$ wavenumbers in each direction, which as before are selected logarithmically spaced within the interval $[0.08, 1.25]$ m^{-1}. With these parameters, 225 pairs of (a_n, b_n) coefficients are calculated in the LSM minimization. As in 1D, the reconstructed free surface based on these values captures well the salient features of the generated ocean surface. The RMS difference between these is $0.029H_s = 0.058$ m over the grid,and it is only $0.021H_s = 0.042$ m when calculated at the LIDAR data points.

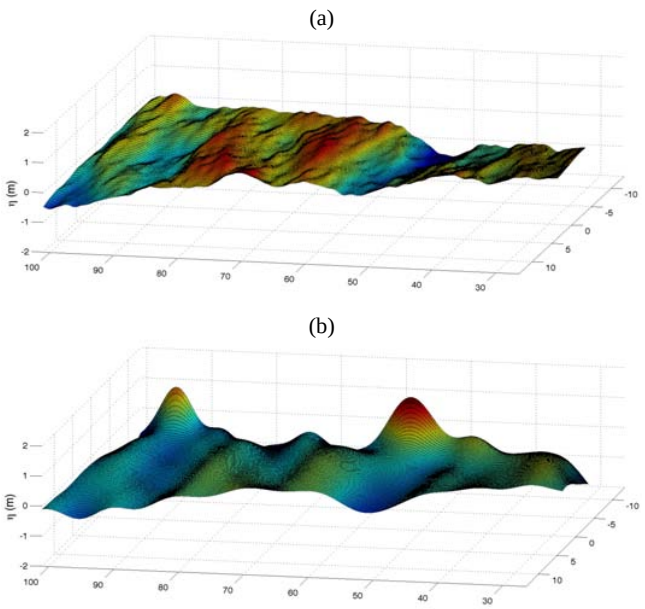

Fig. 7: Same case and parameters as in Fig. 6, at $t = 3.25$ s: (a) direct propagation of ocean surface simulated at $t = 1.25$ (Fig. 6a); and (b) forecast ocean surface on the basis of reconstruction at $t = 1.25$ (Fig. 6b).

A forecast of the generated and reconstructed ocean surfaces is now made, which is shown in Fig. 7, by marching the time variable forward. A rigorous analysis of the predictable area in space-time for a directional wavefield was proposed by Wu (2004), who showed that, for a single probe (i.e., one spatial data point), the maximum predictable time is a function of the slowest and fastest wave components (in terms of group velocity, Eq. (2), i.e., c_g^{min} and c_g^{max}, respectively), that "cross" the initialization period Δt_i (1.25 s here),

$$\Delta t_f = \Delta t_i \, \frac{c_g^{max}}{c_g^{max} - c_g^{min}} \tag{30}$$

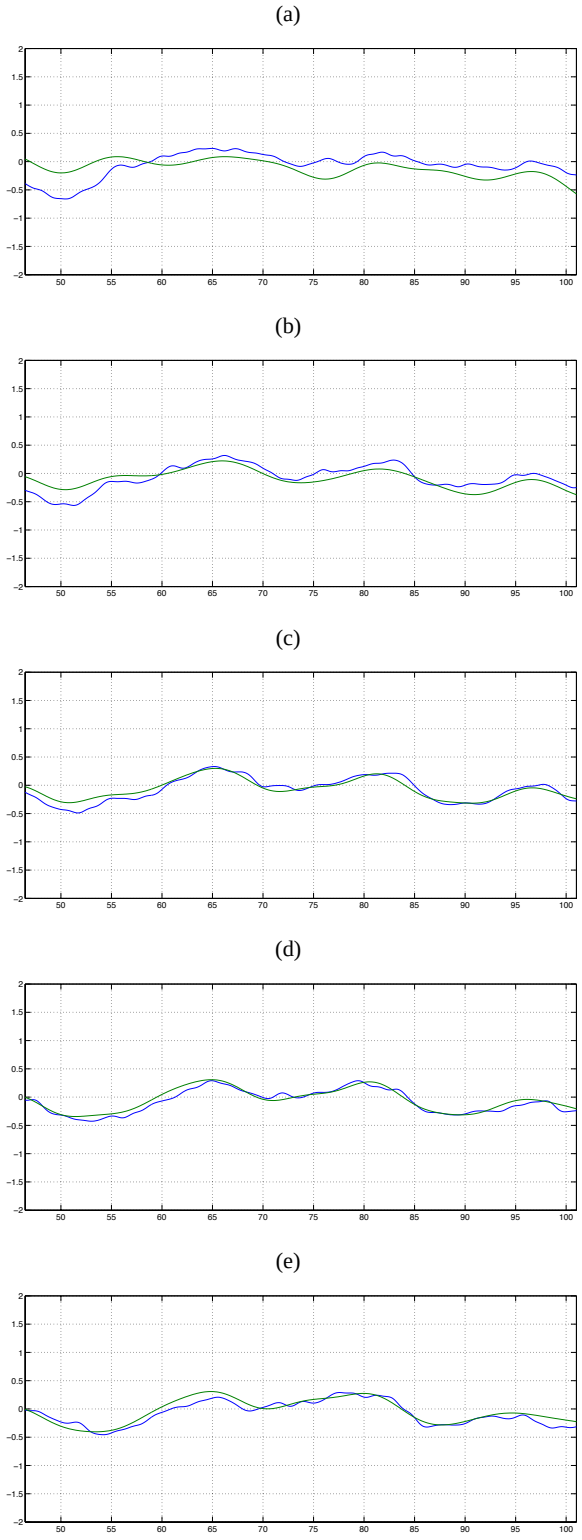

Fig. 8: Case of Fig. 6: 2D vertical slices in data, in a few directions (index: 16,24,32 (middle),40,48) of vertical LIDAR planes. Blue: generated forecast; Green: reconstructed forecast.

The same work also showed how this prediction period can be extended by increasing the number of "wave probes". For $k_n = 0.056 - 0.889$ m^{-1}, the minimum and maximum group velocities of directional wave components are, $c_g^{min} = 1.98$, $c_g^{max} = 26.61$ m/s; hence, the forecast for one probe is limited to $\Delta t_f = 1.35$ s in the future. Although we did not perform any detailed calculation for the large number of spatial "probes" that the intersecting LIDAR rays constitutes, we verify in the following that $\Delta t_f = 2$ s is still at or near the upper bound of what is acceptable for an accurate enough forecast in the selected spatial area. More work is clearly needed to better establish the relevant value of Δt_f as a function of all the problem's parameters.

Thus, Fig. 7a shows the simulated ocean surface of Fig. 6a, propagated to $t_f = \Delta t_i + \Delta t_f = 3.25$ s, and Fig. 7b similarly shows the reconstructed surface of Fig. 6b, propagated to the same time level. [Note, the propagation is simply done by reevaluating the algebraic equations describing the free surface for a different time, but using otherwise the same wavenumbers (k_{nx}, k_{ny}), circular frequencies ω_n and amplitude coefficients (a_n, b_n) as for the reconstruction. Also note, for the simulated surface, there are 6,400 component vectors in the random phase generation based on the JS spectrum with $N = 320$, and for the reconstructed surface, there are only 15 x 15 = 225 component vectors in the present case.] We see that, while the general features of the surface of Fig. 7a are overall well predicted in Fig. 7b, these are no so well predicted near the border of the domain. Because of this the RMS difference between these surfaces on the original distorted grid is larger, at $0.13H_s = 0.26$ m, than for the nowcast at $t = 1.25$, which is to be expected.

A closer inspection of the discrepancies between both surfaces in Fig. 8, however, for a series of vertical cross-sections in the surfaces of Fig. 7, indicates that the agreement between both surfaces is much better along a strip near the middle of the domain, which would likely encompass the path of a vessel traveling in this direction in an actual situation. We clearly see that larger discrepancies only occur near the sides of the domain (in Fig. 7b, mostly at a few spots on the far side). Accordingly the RMS difference between the 2 surfaces on the original distorted grid is reduced, at $0.08H_s = 0.16$ m, when using angular directions for indices 16-48. [Note, if one performs the forecast for $\Delta t_f = 3$ s in the future, the latter error becomes $0.20H_s = 0.4$ m, which is too large. To achieve a more accurate longer term forecast, one would need to use a larger number of time steps/frames than 6.]

CONCLUSIONS

We have shown in this work that both 1D and 2D irregular ocean surfaces can be reconstructed as a *nowcast*, on the basis of unevenly distributed simulated LIDAR observations. Both linear and Choppy free surface generation and reconstruction algorithms were developed and validated. The best results are obtained when the LIDAR data set combines both spatial and temporal data (typically for 5-6 successive frames), which is easy to achieve in practice, considering the fairly high frequency of data acquisition of the anticipated typical LIDAR camera (i.e., 4-20 Hz). In the case of a 2D linear reconstruction using spatio-temporal data, we show that a short term *forecast* of the ocean surface in a fairly wide strip in the main aiming direction of the camera (i.e., also the trajectory of a vessel), can be accurately and efficiently (i.e., analytically) generated.

A larger data set (i.e., in terms of number of LIDAR rays/data points and frames) allows both for a higher-resolution reconstruction of the ocean surface (i.e., using a larger number of wave harmonics, providing a better coverage of the relevant frequency range), and a more accurate reconstruction (in terms of RMS difference with the initial surface), particularly in shadow areas behind wave crests. In such a case, the forecast is also expected to be of better quality and to stay reliable for a longer

term forecast.

Linear or Choppy reconstructions of the ocean surface were performed for both 1D and 2D cases. In the latter case, the use of the efficient iterative solver GMRES allows for a fast and accurate solution in less than 1 s CPU on a standard laptop, without any particular optimization and using the interpreted Matlab software. Clearly, a multiple core or GPU implementation in a compiled language would reduce this time by 1-2 orders of magnitude. This optimization part of the numerical model will take place in future work. The free surface generation and reconstruction based on the Choppy model was only implemented and validated in 1D, and the extension and validation of the 2D-Choppy free surface reconstruction will also be performed in future work. Additionally, future work will also include, the systematic assessment of the sensitivity of results (i.e., free surface reconstruction) to various numerical and model parameters and also to the presence of noise/measurement error in simulated LIDAR data. Importantly, one would also assess the effect of the motion of the vessel, on which the LIDAR camera is mounted, on the spatio-temporal reconstruction of the ocean surface.

Finally, when relevant hardware becomes available in this project, one will start using actual LIDAR data and adapt the various algorithms accordingly, if necessary.

ACKNOWLEDGEMENTS

The first and last authors' research was funded by the Navy STTR Program and managed by the Office of Naval Research, Code 333, contract number N0001410M0277.

REFERENCES

Belmont M.R. (2007). "Application of non-uniform to uniform data mapping to: Shallow angle LIDAR with the introduction of independent variable techniques," *Signal Processing*, Vol 87, pp 2461-2472, doi:10.1016/j.sigpro.2007.04.005.

Belmont,M.R., Horwood R., Thurley W.F., and J. Baker (2006). "A Shallow angle wave profiling Lidar," *J. Atmospheric and Oceanic Tech.*, Vol 24, pp 1150-1156, doi:10.1175/JTECH2032.1.

Blondel E. (2009). *Reconstruction et prévision déterministe de houle à partir de données mesurées*, Ph.D. Dissertation, Ecole Centrale de Nantes.

Blondel E., F. Bonnefoy and P. Ferrant (2010). "Deterministic non-linear wave prediction using probe data," *Ocean Engng.*, Vol 37, pp 913-926, doi:10.1016/j.oceaneng.2010.03.002.

Dean, R.G. and Dalrymple R.A. (1984). *Water Wave Mechanics for Engineers and Scientists*, Prentice-Hall.

Nouguier F., C.-A. Guérin and B. Chapron (2009). "Choppy wave model for Nonlinear Gravity Waves," *J. Geophys. Res.*, Vol. 114, C09012, doi:10.1029/2008JC004984.

Wu G. (2004) *Direct simulation and deterministic prediction of large-scale nonlinear ocean wave-field*, Ph.D. Dissertation, Massachussets Institute of Technology.